Mimicking Bone Nanostructure by Combining Block Copolymer Self-Assembly and 1D Crystal Nucleation

Xi Chen, Wenda Wang, Shan Cheng, Bin Dong, and Christopher Y. Li*

Department of Materials Science and Engineering, Drexel University, 3141 Chestnut Street, Philadelphia, Pennsylvania 19104, United States

ABSTRACT The orientation and spatial distribution of nanocrystals in the organic matrix are two distinctive structural characteristics associated with natural bone. Synthetic soft materials have been used to successfully control the orientation of mineral crystals. The spatial distribution of minerals in a synthetic scaffold, however, has yet to be reproduced in a biomimetic manner. Herein, we report using block copolymer-decorated polymer nanofibers to achieve biomineralized fibrils with precise control of both mineral crystal orientation and spatial distribution. Exquisite nanoscale structural control in biomimetic hybrid materials has been demonstrated.

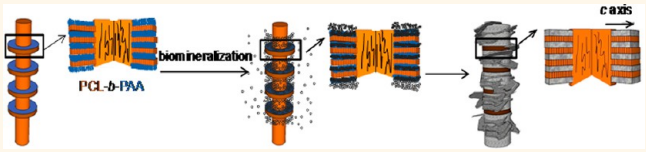

KEYWORDS: bone structure · biomineralization · biomimetics · block copolymer self-assembly · polymer crystallization · nano hybrid shish kebab

Bone is a masterpiece from nature with exceptional load-bearing properties originated from the extensively studied seven-level hierarchical structure, spanning from molecular to macroscopic length scales.[1−3] Despite various macrostructures, morphogenically different bones share similar nanostructures consisting of collagen fibrils within which organized hydroxyapatite (HAP) nanocrystals are embedded. These HAP-collagen hybrid fibrils are the building blocks of a natural bone, and they show unique banding pattern with a period of 67 nm, which arises from the periodically distributed HAPs in self-assembled collagen fibrils. The *c*-axes of the HAP crystals are aligned parallel to the fiber axis. The banding pattern results from preferred nucleation of HAP crystals within the gap zones of collagen fibrils.[4−7] While study on bone mineralization continues, a synthetic alternative to replace bone autografts for treating diseases associated with bone defects has been sought since the 1980s.[8−11] Numerous polymeric materials such as polylactide, polycaprolactone (PCL), and polyhydroxyacid, in fiber or gel forms, have been used for biomineralization.[9] In spite of extensive research efforts, up until now, no synthetic template can induce biomineral growth with controlled mineral orientation and spatial distribution that mimics natural bone. To this end, Stupp *et al.* designed and synthesized self-assembled polypeptide amphiphilic (PA) nanofibers to mimic collagen fibrils.[10] They demonstrated that PA nanofibers are able to control the orientation of HAP crystals with the crystal *c*-axis being parallel to the fiber axis due to the epitaxial relationship between HAP and the PA fiber.[10] However, the spatial distribution of HAP on the PA nanofibers was not controlled; therefore, the banding pattern was not observed. Electrospun nanofibers were also used to template mineral growth with no clear orientation control.[8,12] For biomimetic mineralization, spatial distribution of nanometer sized minerals in the organic fiber matrix is of utter importance because it can directly lead to controlled organic−inorganic interfacial area and mineral contents, both of which are critical for mechanical properties, degradation behavior and possible biocompatibility of the hybrids. Herein, we demonstrate, for the first time, that orientation and spatial distribution of mineral nanocrystals can be precisely controlled on the nanoscale by employing block copolymer self-assembly and one-dimensional (1D) polymer nucleation processes.

Our design aims to mimic the hierarchical structure of natural bone (Scheme 1a) from

* Address correspondence to chrisli@drexel.edu.

Received for review July 19, 2013 and accepted August 23, 2013.

Published online August 24, 2013
10.1021/nn403742f

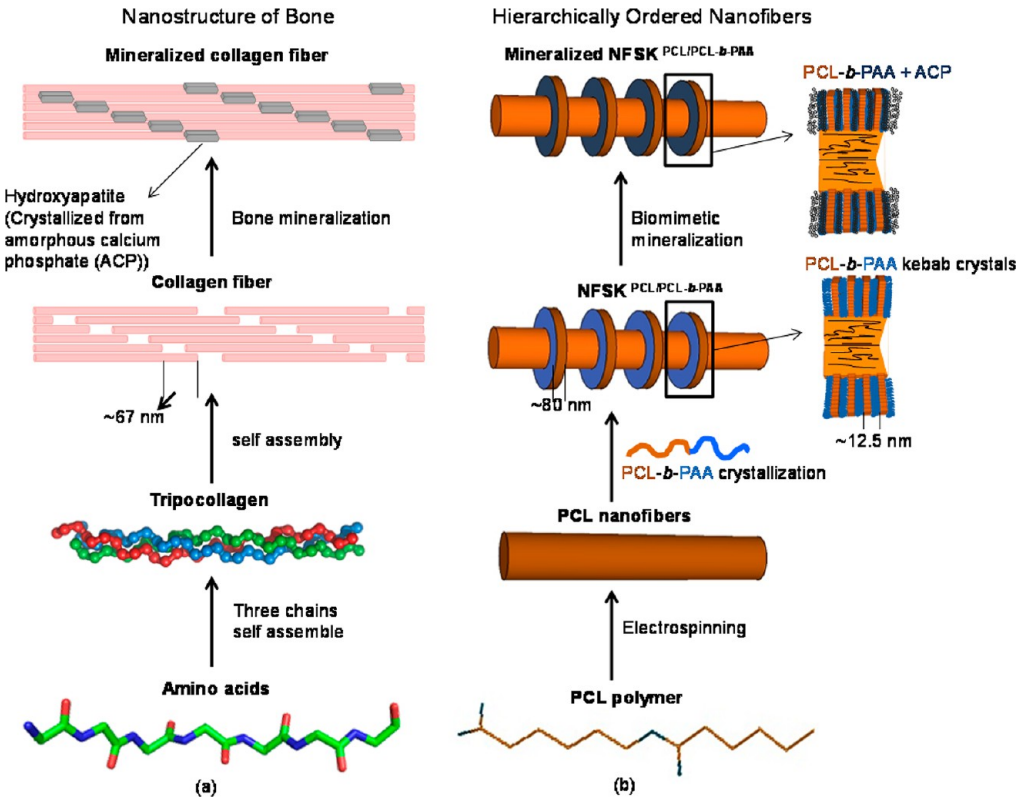

Scheme 1. Comparison of the hierarchical nanostructure of natural bone (a) and the present nanofiber shish kebab design (b). Panel a shows that (from bottom to top) polypeptides assemble to form tripocollagens, which further form collagen fibrils. The latter has negatively charged gap zones periodically distributed in the fibrils, which allow precise control of biomineral spatial distribution. The minerals are confined in the gap zone. Panel b shows that (from bottom to top) polymers (*e.g.*, PCL) can be electrospun into nanosized fibers. Controlled crystallization of a carefully selected block copolymer (*e.g.*, PCL-*b*-PAA) leads to shish kebab type of nanomorphology, where the nanofiber is the shish and the block copolymer forms the crystalline kebab. PCL-*b*-PAA forms the alternating PCL and PAA domains in each kebab with ~12.5 nm spacing (brown and blue). Subsequent mineralization leads to precisely controlled hybrids mimicking natural bone.

the molecular to mineralized collagen fibril level, as shown in Scheme 1a. Since the mineral crystal orientation has been successfully realized in synthetic systems as previously discussed, the novelty of our strategy is incorporating a structural design to control both the orientation and spatial distribution of the mineral on polymeric naonfibers. We combine 1D nucleation and block copolymer self-assembly to achieve this goal. When 1D materials such as carbon nanotubes or polymer nanofibers nucleate the growth of polymer crystals, because of depletion-induced concentration gradient generated by the crystal growth process, the crystal growth follows a (quasi) periodic pattern with the period ranging from a few tens to hundreds of nanometers.[13−15] Using block copolymer self-assembly, we can tune the chemical environment in the vicinity of the polymer single crystals to allow nanoconfined biomineralization, as shown in Scheme 1b. When comparing panels a and b of Scheme 1, the periodic, block copolymer crystal-decorated polymer nanofibers resemble natural collagen fibrils with periodic gap zones. Upon mineralization, if biominerals are formed within the block copolymer domains, the resultant hybrid structure would be remarkably similar to naturally occurring bone in terms of spatial distribution of the mineral. Furthermore, oriented mineral growth may be achieved in the block copolymer nanodomains. To this end, PCL is chosen as the model polymer to form the nanofiber because of its biocompatibility and semicrystalline nature. PCL-*b*-poly(acrylic acid) (PCL-*b*-PAA) block copolymer is used as the model block copolymer because (1) the PCL block is able to crystallize on PCL nanofibers to generate the necessary periodic nanostructure;[16] and (2) the PAA chains form acrylic acid-rich nanodomains (Scheme 1b) that mimic the chemical environment of the gap zones in natural collagen fibrils, and should facilitate mineral formation. Furthermore, the ordered block copolymers can impose nanoconfinement on mineral crystal growth, through which oriented mineral crystals can be obtained.

RESULTS AND DISCUSSION

PCL nanofibers with an average diameter of *ca.* 200 nm were obtained using electrospinning as previously reported (Figure 1a).[16] PCL-*b*-PAA (the synthesis and characterization procedure is detailed in the Supporting Information) was crystallized onto PCL

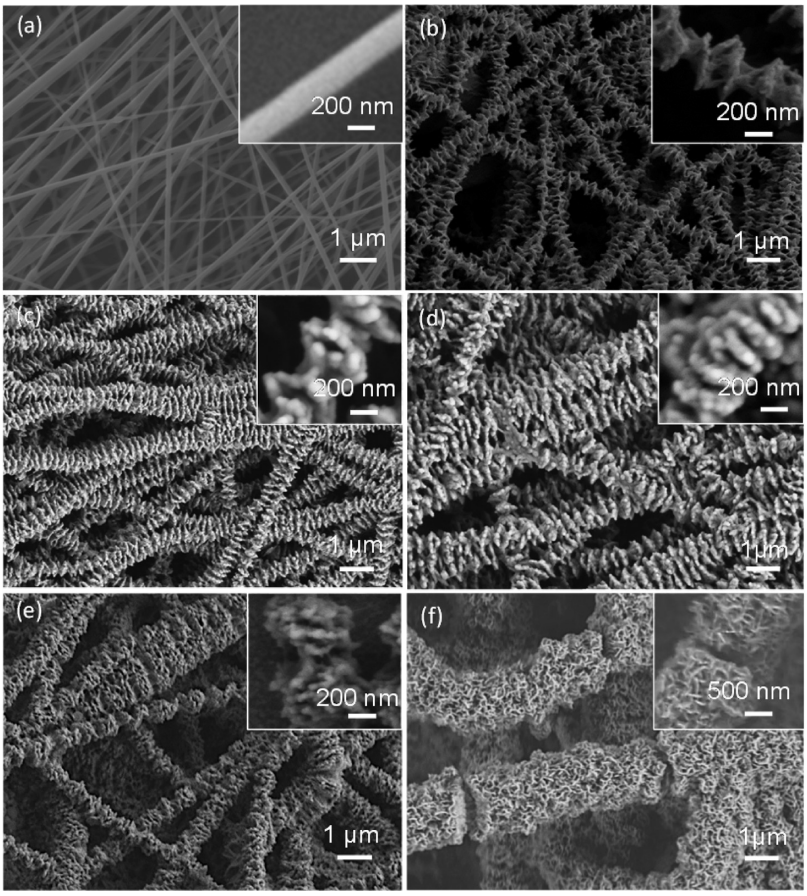

Figure 1. SEM images of (a) PCL nanofibers, (b) NFSKs before mineralization, and (c−f) NFSKs after mineralization for (c) 1, (d) 3, (e) 5, and (e) 7 days.

nanofibers *via* solution incubation as described in the Methods section. Figure 1b and Scheme 1b show the resultant structure: the nanofibers are decorated with lamellar crystals that are orthogonal to the fiber axis, and the lamellar crystals form a quasi-periodic pattern. The overall structure is similar to the classic shish kebab morphology observed in flow-induced polymer crystallization.[17,18] The central fiber can be considered as "shish" and the block copolymer crystals are "kebabs" (Scheme 1b). Nanofiber shish kebab (NFSK) is then used to describe this nanoscale morphology. The kebab period is 193 ± 42 nm and the crystal lateral size is 407 ± 55 nm. The formation mechanism of this unique structure is attributed to soft epitaxy:[18] In a PCL nanofiber, polymer chains are parallel to the fiber axis. As the block copolymer chains start to crystallize on the surface of the nanofiber, although the lattice matching between the PCL fiber and the PCL kebab crystal may not be fulfilled, the PCL segments of the block copolymers do align parallel to the fiber axis. The PAA segments are then excluded onto the surface of the PCL crystal lamellae to form anionic nanodomains, and they also can further facilitate the crystal growth of the adjacent PCL layer.[14] The hierarchical block copolymer NFSK structure is shown in Scheme 1b. The kebabs with anionic nanodomains mimic the gap zones in collagen fibers. Note that the block copolymer domains are not evident from Figure 1b, but lamellar layers within kebabs are clearly illustrated from transmission electron microscopy (TEM) experiments (see later discussion). The PAA segments in NFSKs dramatically change water wetting behavior of the NFSK fiber mat. The pristine PCL nanofiber mat is hydrophobic with a contact angle of 112.7° (Figure S2a). After introducing PCL-*b*-PAA crystals, the contact angle decreases to 43.3° (Figure S2b). This significant decrease in water contact angle should facilitate the NFSK mineralization process.

To perform biomimetic mineralization, we used a two-time concentrated simulated body fluid (2SBF) as the mineralization media.[19−21] Figure 1c−f shows the morphological evolution of mineralized NFSKs after mineralization for 1, 3, 5, and 7 days, respectively. Both calcium and phosphorus elements were detected on the surface of NFSKs after mineralization for 1 day (Figure S3e,f). While nanofibers retained their shape in all the samples, the shish-kebab morphology can only be observed for samples that have experienced no more than 5 days of mineralization. After 7 days of mineralization, a layer of random oriented plate crystals was formed, suggesting overgrowth of minerals (Figure 1f). Note that control experiments on bare PCL nanofibers and NFSKs using a PCL-*b*-poly(*tert*-butyl acrylate) as the kebab

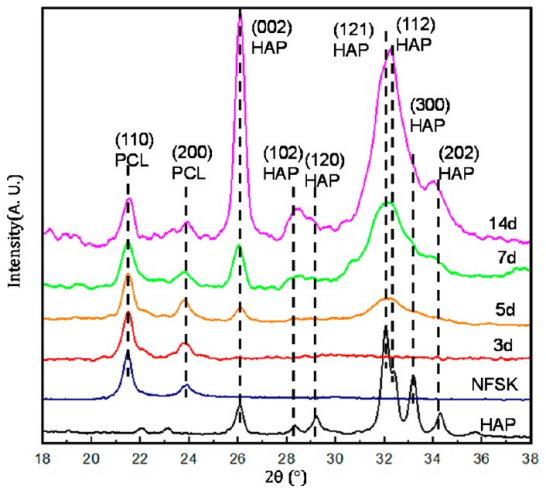

Figure 2. XRD patterns of NFSKs mineralized in 2SBF for 3, 5, 7, and 14 days. The diffraction profiles are normalized to show the same diffraction intensity from (110) plane of PCL crystals. XRD patterns of HAP nanoparticles and NFSKs before mineralization are also shown for comparison.

forming block copolymer without anionic nanodomains in kebabs showed that no mineral can be detected even after mineralizing under the same condition for 14 days (Figure S3a–d), indicating the local anionic PAA nanodomains are critical for biomimetic mineralization.[22]

The structural evolution of the mineralized NFSK was followed using X-ray diffraction (XRD) experiments (Figure 2). NFSK before mineralization showed two distinct diffraction peaks with 2θ at 21.4° and 23.9°, corresponding to (110) and (200) crystalline planes of PCL.[23] The diffraction pattern did not change after up to 3 days of mineralization, confirming the amorphous nature of minerals observed in Figure 1c,d (amorphous calcium phosphate, ACP, as shown in Scheme 1). Diffraction peaks corresponding to HAP crystals were found after 5 days of mineralization, while the PCL diffractions remained unchanged for the sample. The HAP diffraction intensities increased upon further mineralization, due to the increased amount of HAP crystals formed on NFSKs, as confirmed by thermogravimetric analysis (TGA, Figure S4). The mineral contents can be estimated to be ~11, 20, 51, and 77 wt % after 3, 5, 7, and 14-day mineralization, respectively. The crystallization of minerals has also been confirmed using FTIR, detailed in Figure S5 and Table S3. The broad band between 550 and 610 cm^{-1}, associated with amorphous HAP, splits into two bands at 565 and 605 cm^{-1} (Figure S5) upon HAP crystallization, consistent with the XRD results. Bands at around 876, 1500–1600 cm^{-1} for 5-day mineralized NFSKs can be assigned to CO_3^{2-}, indicating that HAP minerals formed in NFSKs are carbonated HAP with phosphate or hydroxyl ions partially substituted by carbonate ions, as commonly observed in natural bones.[24,25]

With the combination of SEM, XRD, and FTIR results, we propose a three-stage growth process for NFSK mineralization: (1) early stage mineralization (days 0–3), when ions are infiltrated into NFSKs to form ACP, which is confined within the PAA nanodomains (Figure 1c,d); (2) intermediate stage mineralization (day 3–5), when the ions continuously infiltrate into the PAA domains while ACP converts to a crystalline form, and the crystalline minerals are confined within the block copolymer domains (Figure 1e); and (3) late stage mineralization (>5 days). As shown in Figure 1f, after more than 5 days of mineralization, excessive mineral crystals are formed and they grow out of the NFSKs. In early and intermediate stages of mineralization, the mineralization process is directed by the kebabs of block copolymer crystals. The process is intra-NFSK, and resembles the intrafibrillar mineralization in natural bones. Although the intrafibrillar mineralization has been known to play an important role in the exceptional properties of bones, to our knowledge, no intrafibrillar mineralization has been reported in mineralization of synthetic polymer fibers. During the late stage of mineralization, because the entire block copolymer domains are filled by mineral crystals, the continuous mineral growth behaves similar to that on smooth nanofiber surface.[12]

TEM was employed to elucidate the spatial distribution and orientation of minerals within NFSKs. Figure 3a indicates that the mineralized NFSKs have a kebab period of ~185 nm, which arises from the crystal formation on the surface of PCL nanofibers. Figure 3b reveals that each "kebab" crystal exhibits a banding pattern: there are ~8 dark/gray alternating layers which are perpendicular to the fiber axis. The banded structure has a period of ~12.5 nm and the contrast arises from the enrichment of minerals in the negatively charged PAA domains; the dark stripes represent PAA blocks in PCL-*b*-PAA, while the light stripes represent PCL single crystals formed during controlled crystallization on PCL nanofiber surface (Figures 3a–c).

Selected area electron diffraction (SAED) experiments show the minerals in the kebabs after 1-day mineralization are amorphous (inset of Figure 3b). Upon mineral crystallization, this banded structure diminishes from the TEM image (Figure 3d,e) and is replaced by plate-like mineral crystals, suggesting the minerals are organized with a preferred orientation along kebab surface. This is significantly different from those formed on electrospun nanofibers reported in literature,[12,19] where spherical mineral clusters are formed. To further demonstrate the mineral crystal orientation, SAED experiments are conducted on single mineralized NFSK as shown in Figure 3f. The diffraction from (002) ($d \sim 3.44$ Å) planes of crystalline HAP forms a pair of arcs in the direction perpendicular to the fiber axis, suggesting that the *c*-axis of HAP is perpendicular to the fiber axis. To illustrate the orientation of minerals in kebabs, 5-day mineralized NFSKs

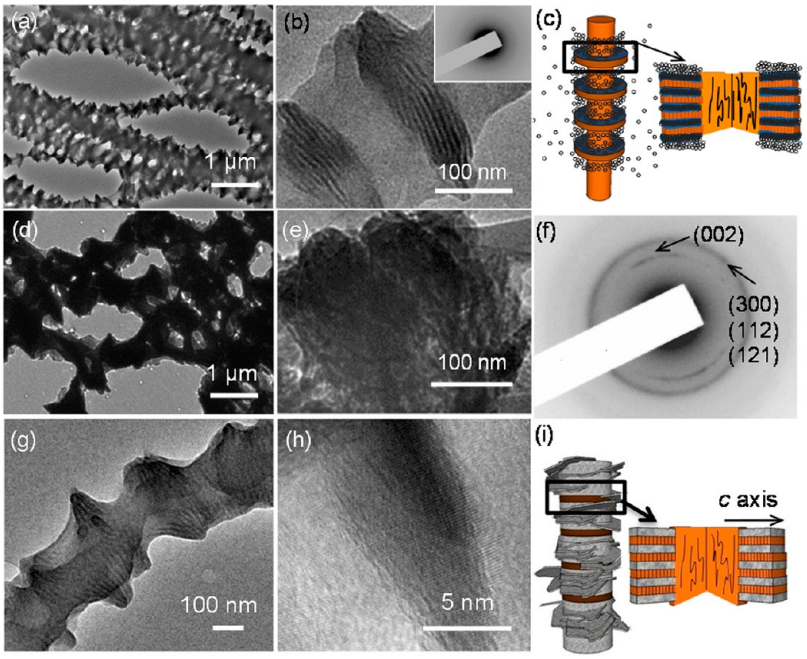

Figure 3. TEM images of NFSKs mineralized for 1 day (a and b) and 5 days (d, e, g, h). Panel b is an enlarged image of (a); inset of (b) shows SAED pattern taken from (b). Panel e is an enlarged image of (d). Panel f shows the SAED pattern from (e) with correct orientation. Panel g shows the interior of (d) obtained by sonicating sample (d) in ethanol for 1 min. Panel h shows a high resolution TEM image of (g). Panels c and i show schematic representations of NFSKs with amorphous and crystalline HAP, respectively.

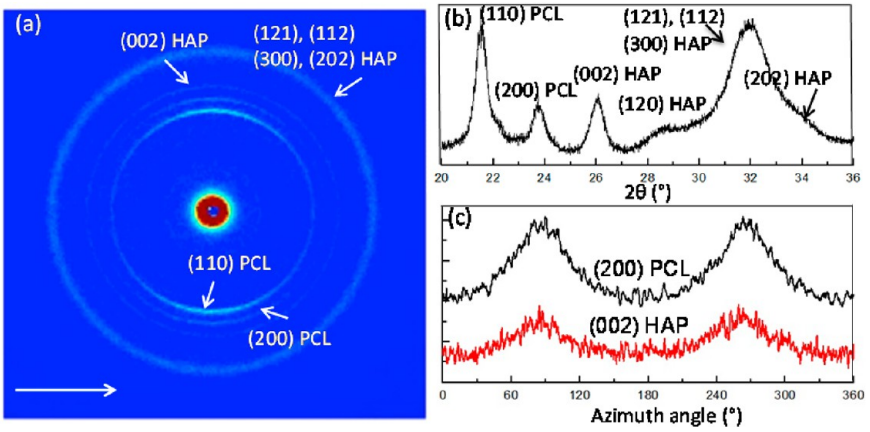

Figure 4. (a) Wide angle X-ray diffraction (WAXD) profile of aligned NFSKs after 5 days of mineralization. (b) Azimuthal integration of (a). (c) Azimuthal profile of WAXD. The profile shows a clearly higher intensity at ~90° and 270° for diffractions from (200) planes of PCL and (002) planes of hydroxyapatite (HAP), which means the *c*-axis of HAP is perpendicular to the *c*-axis of PCL.

shown in Figure 3d were sonicated in ethanol for ~1 min to remove excessive minerals on the surface. After sonication, the NFSKs show a banded structure (Figure 3g), and high resolution TEM image shows that the (002) planes of the crystalline minerals are perpendicular to the kebab surface (Figure 3h). TEM tomography has also been conducted to reveal the 3D nature of the HAP-NFSK hybrid (video, Supporting Information), which confirms that the *c*-axis of HAP is parallel to the kebab surface.

The preferred orientation of HAP in NFSKs is further confirmed with two-dimensional wide-angle X-ray diffraction (WAXD) using aligned NFSKs after 5 days of mineralization, and the diffraction pattern is shown in Figure 4a. Fiber axis is along the equator direction. The diffractions from HAP ($2\theta = 25.9°, 32°$) can be assigned to (002) and a complex of (121), (112) and (300) crystalline planes, which are consistent with the diffractions of carbonated apatites in natural bones.[26,27] Diffractions at $2\theta = 21.5°$ and 23.8° correspond to (110) and (200) planes of PCL, respectively (Figure 4a,b). Figure 4c shows the azimuthal profile of (200) planes of PCL and (002) planes of HAP, both depicting high intensities at ~90° and 270° azimuthal angles. This clearly indicates the *c*-axis of HAP is perpendicular to the *c*-axis of PCL crystals, which is also the fiber axis.

In bone mineralization, the parallel organization of HAP along collagen fibrils has been ascribed to the

epitaxial relationship at the organic–inorganic interface.[28,29] In this study, the *c*-axes of HAP crystals are perpendicular to the nanofiber axis and we attribute the preferential growth of HAP crystals along the kebabs to the geometrical confinement of the block copolymer lamellae in nano scale and a faster growth rate along *c*-axis. Soft matter-, particularly block copolymer-confined mineral growth has been reported.[30,31] The 2D PAA nanodomains in our case are confined between PCL layers and guide the mineral crystal growth. When mineralization proceeds to the late stage of mineralization, this geometrical confinement no longer exists because the mineral nanocrystals grow out of the block copolymer region, and the orientation of HAP diminishes. Compared to collagen and PA nanofibers that have been widely used for mineralization study, electrospun nanofibers are easy to fabricate and scale up. It is however difficult to precisely manipulate the spatial distribution of charges on nanofiber surface. Controlled crystallization of ionic block copolymer on nanofibers creates not only a periodicity comparable to the banded structure in mineralized collagen fibrils, but also a negatively charged domain to control the spatial distribution and orientation of minerals formed in biomimetic mineralization. Changing block copolymer molecular weight may also allow detailed morphological and structural control of the biomineralization process.

CONCLUSION

In summary, we have demonstrated a new structural design to mimic the natural bone nanostructure by combining self-assembly of ionic block copolymers and 1D polymer crystallization. Electrospun PCL nanofibers are used to induce crystallization of ionic block copolymer PCL-*b*-PAA and a unique block copolymer NFSK nanostructure is formed. Within each kebab, block copolymer assembly leads to ionic PAA nanodomains which mediate HAP mineral growth. Carbonate HAP minerals grow along kebabs with their *c*-axes parallel to the kebab surface due to the geometrical confinement between two adjacent PCL-*b*-PAA lamellar crystals. For the first time, precisely controlled HAP mineral orientation and distribution are achieved in a synthetic polymer system. We anticipate that our approach will provide a new route for biomimetic design of hybrid materials in general and bone mimics in particular.

METHODS

The Formation of NFSK Structure. PCL nanofibers were prepared by electrospinning 12% PCL (80 000 g/mol, Sigma Aldrich) in trifluoroethanol (NMR grade, Sigma Aldrich) at 18 kV with a flow rate of 0.3 mL/h, and collected at a distance of 13 cm from the spinneret. PCL nanofiber mats were then immersed in 1% PCL-*b*-PAA in mixed solvent of pentyl acetate and ethanol (1:1 w/w) for 1 h and washed with the mixed solvent three times to remove the free block copolymers on the surface of the fiber mat. Samples were then dried under vacuum overnight to remove the residue solvent.

Biomimetic Mineralization of NFSKs. A 1 cm × 1 cm NFSK mat was incubated in ~10 mL of concentrated SBF (2SBF, preparation and ion concentrations were detailed in Supporting Information). The mineralization solution was filtered through a membrane with 0.2 μm pores before mineralization and the solution was refreshed every 2 days to compensate the consumption of ions during mineralization. Samples were washed with distilled water and dried in vacuum overnight before characterization.

Characterization. SEM (Zeiss Supra 50VP) samples were coated with carbon before characterization to increase the conductivity without affecting EDS (Oxford) profiles. For TEM (JEOL JEM2100) characterization, mineralized NFSKs were freeze fractured in liquid nitrogen and dispersed in ethanol, followed by solvent casting on a carbon-coated TEM grid.

For WAXD (Rigaku S-MAX 3000) characterization, NFSK mats with aligned nanofibers were mounted between two kapton foils. The aligned nanofibers were prepared by collecting nanofibers on parallel copper wires. The X-rays were generated by a copper target operated at 45 kV/0.88 mA. By inserting an image plate with a 10 mm slit at the center between sample and small-angle X-ray scattering detector, we could collect wide-angle diffraction data (2D X-ray diffraction). For FTIR experiments performed on Varian Excalibur FTS-3000, mineralized NFSKs were mixed with potassium bromide and pressed into pellets. Spectra were collected with a 4 cm^{-1} resolution after 128 scans. TGA was performed using a Perkin-Elmer TGA-7 purged with dry air at 20 mL/min. Approximately 2–3 mg samples were used in TGA experiments to heat from 30 to 800 °C at 10 °C/min and annealed at 800 °C for another 60 min.

Conflict of Interest: The authors declare no competing financial interest.

Supporting Information Available: Detailed experimental procedures, TEM tomography, NMR and FTIR data. This material is available free of charge *via* the Internet at http://pubs.acs.org.

Acknowledgment. This work was supported by the National Science Foundation grant DMR-1308958.

REFERENCES AND NOTES

1. Weiner, S.; Wagner, H. D. The Material Bone: Structure Mechanical Function Relations. *Annu. Rev. Mater. Sci.* **1998**, *28*, 271–298.
2. Fratzl, P.; Weinkamer, R. Nature's Hierarchical Materials. *Prog. Mater. Sci.* **2007**, *52*, 1263–1334.
3. Weiner, S.; Traub, W. Bone Structure: From Angstroms to Microns. *FASEB J.* **1992**, *6*, 879–885.
4. Weiner, S.; Arad, T.; Traub, W. Crystal Organization in Rat Bone Lamellae. *FEBS Lett.* **1991**, *285*, 49–54.
5. Weiner, S.; Traub, W. Organization of Hydroxyapatite Crystals within Collagen Fibrils. *FEBS Lett.* **1986**, *206*, 262–266.
6. Wang, Y.; Azais, T.; Robin, M.; Vallee, A.; Catania, C.; Legriel, P.; Pehau-Arnaudet, G.; Babonneau, F.; Giraud-Guille, M. M.; Nassif, N. The Predominant Role of Collagen in the Nucleation, Growth, Structure and Orientation of Bone Apatite. *Nat. Mater.* **2012**, *11*, 724–733.
7. He, G.; Dahl, T.; Veis, A.; George, A. Nucleation of Apatite Crystals *in Vitro* by Self-Assembled Dentin Matrix Protein 1. *Nat. Mater.* **2003**, *2*, 552–558.
8. Yoshimoto, H.; Shin, Y. M.; Terai, H.; Vacanti, J. P. A Biodegradable Nanofiber Scaffold by Electrospinning and Its Potential for Bone Tissue Engineering. *Biomaterials* **2003**, *24*, 2077–2082.
9. Palmer, L. C.; Newcomb, C. J.; Kaltz, S. R.; Spoerke, E. D.; Stupp, S. I. Biomimetic Systems for Hydroxyapatite

Mineralization Inspired by Bone and Enamel. *Chem. Rev.* **2008**, *108*, 4754–4783.
10. Hartgerink, J. D.; Beniash, E.; Stupp, S. I. Self-Assembly and Mineralization of Peptide-Amphiphile Nanofibers. *Science* **2001**, *294*, 1684–1688.
11. Shin, S. H.; Purevdorj, O.; Castano, O.; Planell, J. A.; Kim, H. W. A Short Review: Recent Advances in Electrospinning for Bone Tissue Regeneration. *J. Tissue Eng.* **2012**, *3*, 2041731412443530-1–11.
12. Chen, J.; Chu, B.; Hsiao, B. S. Mineralization of Hydroxyapatite in Electrospun Nanofibrous Poly(L-lactic acid) Scaffolds. *J. Biomed. Mater. Res.* **2006**, *79A*, 307–317.
13. Laird, E. D.; Li, C. Y. Structure and Morphology Control in Crystalline-Polymer/Carbon-Nanotube Composites. *Macromolecules* **2013**, *46*, 2877–2891.
14. Li, B.; Li, L.; Wang, B.; Li, C. Y. Alternating Patterns on Single-Walled Carbon Nanotubes. *Nat. Nanotechnol.* **2009**, *4*, 358–362.
15. Wang, B. B.; Li, B.; Xiong, J.; Li, C. Y. Hierarchically Ordered Polymer Nanofibers *via* Electrospinning and Controlled Polymer Crystallization. *Macromolecules* **2008**, *41*, 9516–9521.
16. Chen, X.; Dong, B.; Wang, B. B.; Shah, R.; Li, C. Y. Crystalline Block Copolymer Decorated, Hierarchically Ordered Polymer Nanofibers. *Macromolecules* **2010**, *43*, 9918–9927.
17. Pennings, A.; Kiel, A. Fractionation of Polymers by Crystallization from Solution. III. On the Morphology of Fibrillar Polyethylene Crystals Grown in Solution. *Colloid Polym. Sci.* **1965**, *205*, 160–162.
18. Li, L.; Li, C. Y.; Ni, C. Y. Polymer Crystallization-Driven, Periodic Patterning on Carbon Nanotubes. *J. Am. Chem. Soc.* **2006**, *128*, 1692–1699.
19. Rodriguez, K.; Renneckar, S.; Gatenholm, P. Biomimetic Calcium Phosphate Crystal Mineralization on Electrospun Cellulose-Based Scaffolds. *ACS Appl. Mater. Interfaces* **2011**, *3*, 681–689.
20. Prieto, S.; Shkilnyy, A.; Rumplasch, C.; Ribeiro, A.; Arias, F. J.; Rodriguez-Cabello, J. C.; Taubert, A. Biomimetic Calcium Phosphate Mineralization with Multifunctional Elastin-Like Recombinamers. *Biomacromolecules* **2011**, *12*, 1480–1486.
21. Bigi, A.; Boanini, E.; Panzavolta, S.; Roveri, N. Biomimetic Growth of Hydroxyapatite on Gelatin Films Doped with Sodium Polyacrylate. *Biomacromolecules* **2000**, *1*, 752–756.
22. Tay, F. R.; Liu, Y.; Kim, Y. K.; Dai, L.; Li, N.; Khan, S. O.; Pashley, D. H. Hierarchical and Non-Hierarchical Mineralisation of Collagen. *Biomaterials* **2011**, *32*, 1291–1300.
23. Bittiger, H.; Marchessault, R. H.; Niegisch, W. D. Crystal Structure of Poly-[epsilon]-caprolactone. *Acta Crystallogr., B* **1970**, *26*, 1923–1927.
24. Pecile, A.; De Bernard, B. Bone Regulatory Factors: Morphology, Biochemistry, Physiology, and Pharmacology; Plenum Press: New York, 1990.
25. Paschalis, E. P.; DiCarlo, E.; Betts, F.; Sherman, P.; Mendelsohn, R.; Boskey, A. L. FTIR Microspectroscopic Analysis of Human Osteonal Bone. *Calcif. Tissue Int.* **1996**, *59*, 480–487.
26. LeGeros, Z. R. Apatites in Biological Systems. *Prog. Cryst. Growth Charact.* **1981**, *4*, 1–45.
27. Thomas, W. C., Jr.; Tomita, A. Mineralization of Human and Bovine Tissue *in Vitro*. *Am. J. Pathol.* **1967**, *51*, 621–628.
28. Wang, F. K.; Cao, B. R.; Mao, C. B. Bacteriophage Bundles with Prealigned Ca^{2+} Initiate the Oriented Nucleation and Growth of Hydroxylapatite. *Chem. Mater.* **2010**, *22*, 3630–3636.
29. Hoang, Q. Q.; Sicheri, F.; Howard, A. J.; Yang, D. S. C. Bone Recognition Mechanism of Porcine Osteocalcin from Crystal Structure. *Nature* **2003**, *425*, 977–980.
30. Chen, S. F.; Yu, S. H.; Wang, T. X.; Jiang, J.; Colfen, H.; Hu, B.; Yu, B. Polymer-Directed Formation of Unusual $CaCO_3$ Pancakes with Controlled Surface Structures. *Adv. Mater.* **2005**, *17*, 1461–1465.
31. Yu, S. H.; Colfen, H. Bio-Inspired Crystal Morphogenesis by Hydrophilic Polymers. *J. Mater. Chem.* **2004**, *14*, 2124–2147.